CHEMISTRY
A European Journal

A Journal of
ChemPubSoc Europe

Accepted Article

Title: Rhodium-catalysed [2+2+2] cycloaddition reactions of linear allene-ene-ynes to afford fused tricyclic scaffolds. Insights into the mechanism

Authors: Daniel Cassú, Teodor Parella, Miquel Solà, Anna Pla-Quintana, and Anna Roglans

To be cited as: *Chem. Eur. J.* 10.1002/chem.201703194

Link to VoR: http://dx.doi.org/10.1002/chem.201703194

Supported by
ACES

WILEY-VCH

CHEMISTRY
A EUROPEAN JOURNAL

FULL PAPER

DOI: 10.1002/chem.200((will be filled in by the editorial staff))

Rhodium-catalysed [2+2+2] cycloaddition reactions of linear allene-ene-ynes to afford fused tricyclic scaffolds. Insights into the mechanism

Daniel Cassú,[a] Teodor Parella,[b] Miquel Solà,*[a] Anna Pla-Quintana,*[a] and Anna Roglans*[a]

Abstract: Allene-(*E*)-ene-yne *N*-tosyl tethered substrates **3a-3h** were efficiently prepared and their rhodium-catalyzed [2+2+2] cycloaddition reaction was evaluated. The cycloaddition is chemoselective as only the proximal double bond of the allene reacted to afford an exocyclic double bond in the fused tricyclic scaffold. The stereoselectivity depended on the catalytic system used. The comparison of reactivity between allene, alkene and alkyne was studied for the first time by density functional theory calculations. This mechanistic study determines th order in which the unsaturations tak part in the catalytic cycle.

Keywords: cycloaddition • density functional calculations • allenes • reaction mechanisms • rhodium

Introduction

The development of efficient and sustainable syntheses for organic molecules of all shapes and sizes is having a tremendous impact on a wide range of scientific areas, including biomedicine and the production of new drugs, agrochemical products and new materials. The transition metal-catalysed [2+2+2] cycloaddition reaction of three unsaturated partners[1] offers efficient, atom-economical pathways to a variety of complex carbo- and heterocyclic derivatives.

Among the range of unsaturations that can be involved in [2+2+2] cycloadditions, allenes[2,3] have shown great versatility.[4] They are less reactive than alkynes, but allow sp^3 containing six-membered rings to be constructed, opening the door to the enantioselective synthesis of compounds with central chirality. Furthermore, after cycloaddition there is still one unreacted double bond that can be used in subsequent reactions. Despite the progress achieved in this field,[4] there is still room for improvement, especially regarding the control of selectivity. By obtaining a better understanding of aspects governing the selectivity of these processes, we should be able to apply rational criteria to improve them.

[a] D. Cassú, Prof. Dr. M. Solà, Dr. A. Pla-Quintana, Prof. Dr. A. Roglans
Institut de Química Computacional i Catàlisi (IQCC) and Departament de Química
Universitat de Girona (UdG)
Facultat de Ciències, C/ Maria Aurèlia Capmany, 69, 17003-Girona (Spain)
Fax: (+) 34 972 41 81 50
E-mail: anna.roglans@udg.edu

[b] Dr. T. Parella
Servei de Ressonància Magnètica Nuclear
Universitat Autònoma de Barcelona (UAB)
08193 Cerdanyola, Barcelona (Spain)

Supporting information for this article is available on the WWW under http://www.chemeurj.org/ or from the author.

Our research group has explored the rhodium-catalyzed [2+2+2] cycloaddition reaction of linear allene-ene-allene and allene-yne-allene derivatives.[5] The Wilkinson's complex was able to promot the cycloaddition chemoselectively, involving only the interna double bonds of the two allenes, and diastereoselectively.[5a] Th reaction mechanism was studied for the allene-ene-allene substrat by means of DFT calculations. The process involved an initia oxidative addition between the proximal double bond of the allen and the alkene, forming a *cis* ring fusion. Although allenes are mor reactive than alkenes in [2+2+2] cycloaddition reactions entropically favoured allene-alkene oxidative addition was preferre Furthermore, the proximal double bond of the allene, which has molecular orbital with greater energy, was selectively reacted in thi first step. The reaction continued by the insertion of the proxima double bond of the second allene unit to afford a rhodacycloheptan intermediate that evolved, by reductive elimination, to the fina cyclohexane adduct. When optically active substrates, bearing substituent in the α-position of the allene, were reacted under th Wilkinson's complex catalysis, a highly diastereoselective reactio occurred resulting in the production of enantiomerically pur polycycles.[5b]

Since the chemoselectivity of the [2+2+2] cycloadditio reaction is especially compromised when three differen unsaturations are combined in a reaction, we were interested i studying [2+2+2] cycloaddition reactions using the three different carbon-based unsaturations – an allene, an alkene and an alkyne – together. Only two previous examples have been reported evaluating this type of processes (Scheme 1), both in a completely intramolecular manner. Saito, Sato et al.[6] have described the [Cp*RuCl(cod)]-catalysed completely intramolecular [2+2+2] cycloaddition reaction of allene-yne-enes, which diastereoselectively affords fused-tricyclic skeletons with two stereogenic centres. Mukai et al.[7] have reported the stereospecific and stereoselective $[RhCl(CO)_2]_2$-catalyzed intramolecular [2+2+2] cycloaddition of linear yne-allene-ene derivatives to produce

10.1002/chem.201703194

polycyclic products with three contiguous stereogenic centres. In both studies,[6,7] a plausible mechanism is proposed involving oxidative addition between the allene and the alkyne, which are in contiguous – and thus entropically favoured – positions in the linear substrate.

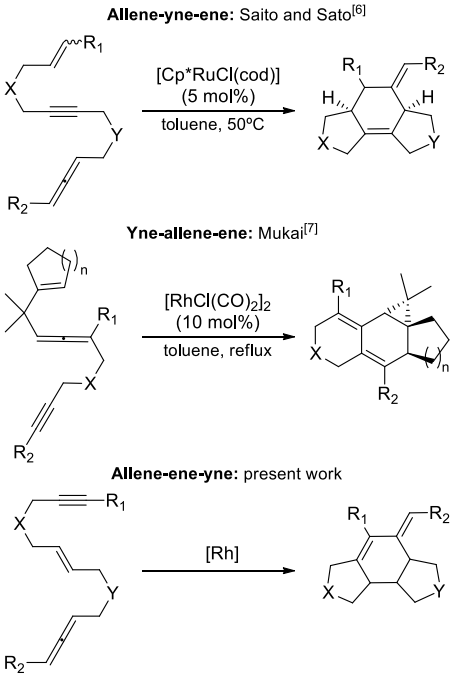

Scheme 1. Transition-metal catalysed [2+2+2] cycloaddition reactions of allenes, alkynes and alkenes.

In the course of our ongoing programme based on the synthesis of polycyclic structures,[8] we designed the present project aimed at reacting allene-ene-yne substrates in which the oxidative addition of the alkyne and the allene is not geometrically favoured (Scheme 1). Apart from the synthetic interest in the tricyclic scaffolds with three contiguous stereogenic centres that can be synthesized, we also wanted to study the process mechanistically, paying special attention to the order of reactivity of the three unsaturations in the [2+2+2] cycloaddition reaction.

Results and Discussion

Synthesis of allene-ene-yne substrates: In order to evaluate the reactivity of allene-ene-yne scaffolds in the completely intramolecular [2+2+2] cycloaddition reaction, a synthesis for eight model substrates **3** was designed. This was based on the nucleophilic substitution of bromoallyl derivatives **1** with N-tosylallenes **2** using potassium carbonate as a base in refluxing acetonitrile (Scheme 2). Variations were introduced at the tether (N-tosyl (NTs) or oxygen (O)) and either at the terminal position of the triple bond (R_1 = H, Me, Et) or the allene (R_2 = H, ^{i}Pr, Ph), or both (Scheme 2) (see SI for details on the synthesis of **3**).

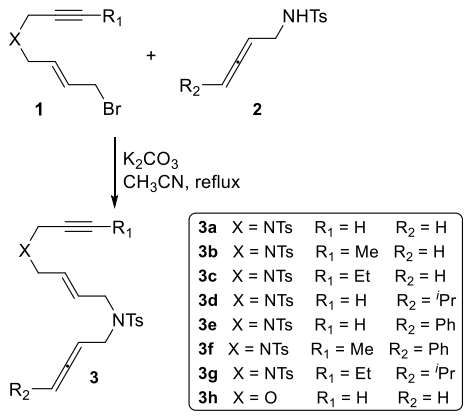

Scheme 2. Allene-ene-yne substrates used in this study (NTs = *p*-toluenesulfonyl).

Cycloaddition reactions: After preparation of the substrates the feasibility of the cycloaddition was assessed with allene-ene-yn **3a** (Table 1). The substrate was first treated with the Wilkinson' catalyst (**A**) in toluene at 100°C. A mixture of two inseparabl diastereoisomers in 8:2 ratio was isolated with an overall 56% yiel (Entry 1, Table 1). The reaction was completely chemoselectiv with cycloaddition taking place only on the internal double bond c the allene. The two diastereoisomers differ in the 6:5 ring fusion that can either be *syn* or *anti* (relative orientation of H_a and H_b i Figure 1). After a complete chemical shift assignment (see SI), i could be inferred that the protons placed in *syn* orientation display smaller coupling constant ($^3J_{Ha\text{-}Hb}$ = 5.6 Hz) than in the *ant* orientation ($^3J_{Ha\text{-}Hb}$ = 10 Hz) (Figure 1), which provided straightforward identification of the two diastereoisomers.

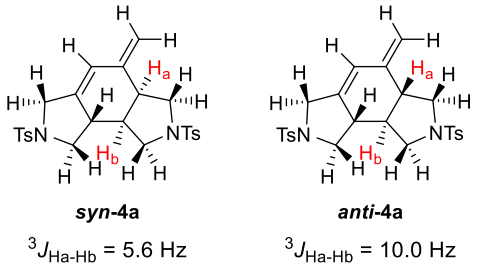

Figure 1. Cycloadducts obtained upon [2+2+2] cycloaddition of allene-ene-yne **3** showing the characteristic coupling constants between H_a and H_b in the tw diastereoisomers.

Ethanol was tested as the reaction solvent to provide a mor polar media (Entry 2, Table 1), but it only caused the degradation o the substrate. *p*-Xylene was also tested to increase the reactio temperature to 130 °C. However, due to decomposition processe the yield of the cycloadduct was lower (Entry 3, Table 1). Given tha no improvement could be achieved by changing the reaction media, further optimization was again attempted in toluene. Neither the use of a microwave heating source, nor the addition of $AgBF_4$ to the reaction mixture to render the catalytic system cationic, led to any improvement. The addition of an excess of triethylamine[8i, 9] to stabilize the catalyst or generate more active species also proved unsuccessful (Entry 4, Table 1).

10.1002/chem.201703194

Table 1. Optimization of the [2+2+2] cycloaddition of **3a**[a]

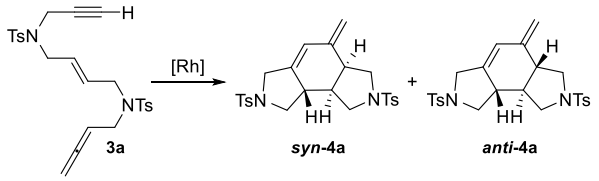

Entry	Catalytic system	Solvent, T (ºC), time	Yield (%) **4**[b]	d.s.[b] syn:anti
1	**A**: $RhCl(PPh_3)_3$	toluene, 100ºC, 5h	56[c]	8:2
2	**A**	ethanol, 70ºC, 22 h	0	---
3	**A**	*p*-xylene, 130ºC, 2.5h	36	10:0
4	**A** Et_3N, 1.8 eq	toluene, 100ºC, 4h	33	9:1
5	**B**: $[Rh(cod)_2]BF_4$ *(R)*-DTBM-SegPhos[d]	dichloroethane, 60ºC, 5h	31	7:3
6	**B**	dichloroethane, 80ºC, 4h	22	5:5
7	**C**: $[RhCl(CO)_2]_2$	toluene, 0-5ºC, 1h	38	0:10
8	**C**	toluene, 60ºC, 20 min	49	1:9

[a] A solution of the catalytic system (10 mol %) was added to **3a** (0.03 M) and the reaction was heated to the temperature noted in the table. [b] The two diastereoisomers were obtained as an inseparable mixture and their ratio was determined by ^{1}H-NMR. [c] 8% of starting material was recovered at the end of the reaction. [d] (*R*)- DTBM-SegPhos stands for (*R*)-(−)-5,5′-bis[di(3,5-di-*tert*-butyl-4-methoxyphenyl)phosphino]-4,4′-bi-1,3-benzodioxole.

The combination of bisphosphine ligands and a cationic rhodium source was then studied as the catalytic system for the cycloaddition of **3a**. Phosphines such as (*R*)-H_8-BINAP, (*R*)-BINAP, and (*R*)-tol-BINAP in combination with cationic rhodium complex $[Rh(cod)_2]BF_4$ were tested in several solvents (dichloroethane and chlorobenzene) and temperatures were raised from room temperature to 100ºC but in no cases did a reaction take place. However, when (*R*)-DTBM-SegPhos was tested in dichloroethane at 60ºC, cycloaddition took place giving a 31% yield of the ***syn*-4a**:***anti*-4a** diastereoisomeric mixture in a 7:3 ratio (Entry 5, Table 1). Lower yields of the cycloadducts **4** were obtained with lower diastereoselectivities when the reaction temperature was increased (Entry 6, Table 1). We also checked the enantioselectivity of the process using chiral HPLC. Unfortunately, no enantioinduction was obtained for the major diastereoisomer ***syn*-4a** and consequently the enantioselectivity study was abandoned.

The dimeric rhodium complex $[RhCl(CO)_2]_2$ (**C**) was then tested in our model cycloaddition reaction to see the effect of a change from phosphine to carbonyl ligands on rhodium. By running the reaction in toluene at different temperatures (Entries 7 and 8, Table 1), the diastereoisomeric mixture of cycloadducts **4a** was efficiently obtained. Surprisingly, the cycloadduct with an *anti* 5,6-ring fusion (***anti*-4a**) was now the major diastereoisomer formed. The yield increased with the temperature but concurred with a slight decrease in the diastereoselectivity. Further increase in the temperature did not improve the reaction.

Since the rhodium sources gave complementary results in terms of selectivity, we decided to check the scope of the process using the three catalytic systems. The optimized conditions found for each catalytic system were applied to the array of allene-ene-yne scaffolds synthesized (Scheme 3).

All compounds except for **3f** react in the cycloisomerization reaction at least under the influence of one of the catalysts tested. The lack of reaction of **3f** is unexplained since **4g**, which was also substituted both in the alkyne and allene ends, reacted with great efficiency. The best results in terms of yields were obtained for the substrate featuring an *i*-propyl substituent at the allene end (**3d** and **3g**). When comparing the results for the three different catalytic systems, it is seen that the neutral rhodium catalytic systems (**A** and **C**) react more efficiently than the cationic one (**B**), which only affords moderate yields of the cycloadducts that are substituted only in the alkyne (**4b** and **4c**) or allene (**4d** and **4e**) terminus. The substrates substituted at both ends (**3f** and **3g**) as well as the one with an oxygen tether (**3h**) failed to react under the catalysis of a mixture of $[Rh(cod)_2]BF_4$ and (*R*)-DTBM-SegPhos, most likely due to steric hindrance.

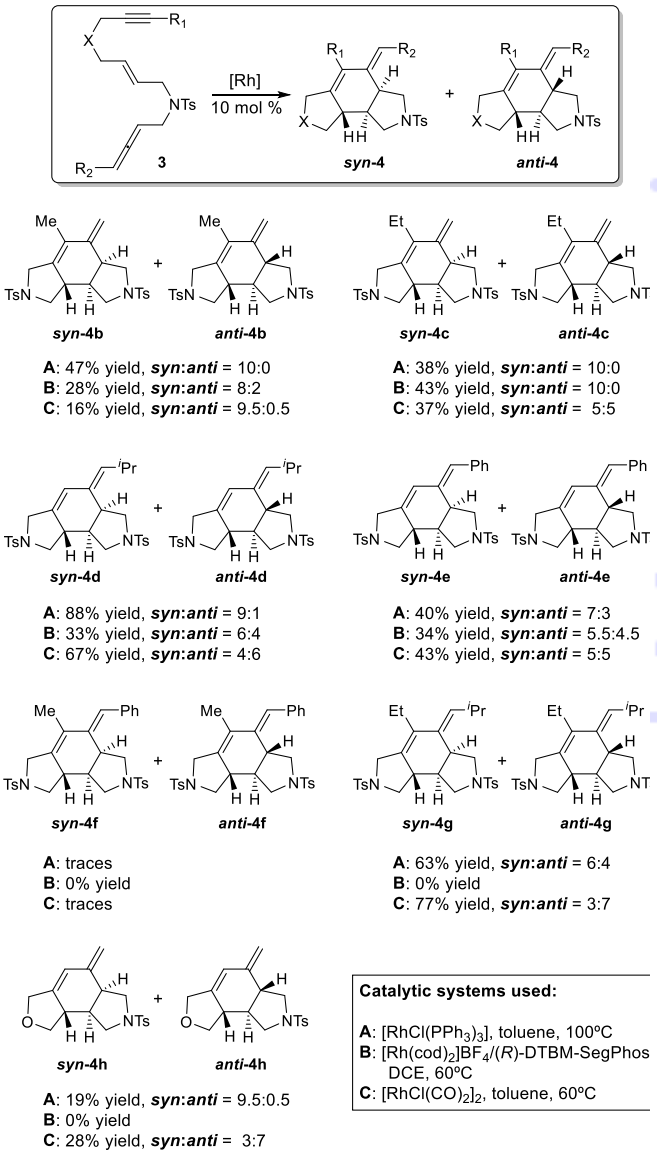

Scheme 3. Scope of the [2+2+2] cycloaddition reactions of substrates **3** (the resul reported are an average of two runs).

As a general trend, Wilkinson's catalyst (catalytic system **A**) displays a higher selectivity for the *syn* cycloadduct. When methyl and ethyl substituents were placed at the terminus of the alkyne group (**4b** and **4c**), pure *syn* diastereoisomers were obtained in moderate yields. It seems that stereoselectivity is reduced when the steric hindrance of the groups on the unsaturation ends is increased. On the other hand, the $[RhCl(CO)_2]_2$ is only moderately selective towards the *anti* cycloadduct in most of the cases, although there are a couple of exceptions. As noted before (Entry 9, Table 1) it is highly selective towards the *anti*-**4a** when the unsubstituted

10.1002/chem.201703194

substrate **3a** is reacted and, quite surprisingly, is highly selective for the *syn*-**4b** cycloadduct when a methyl substituent is placed in the alkyne terminus (**3b**).

Mechanistic study: After exploring the reactivity of the allene-ene-yne substrates from the experimental point of view, we decided to investigate computationally the reaction mechanism of the [2+2+2] cycloaddition reaction of **3a** catalysed by $RhCl(PPh_3)_3$] and $[RhCl(CO)_2]_2$ to yield diastereoisomers *syn*-**4a** and *anti*-**4a**. To this end, we performed density functional theory (DFT) calculations at the B3LYP-D3/cc-pVDZ-PP level (see Computational Methods for more details).

The mechanism postulated for the [2+2+2] cycloaddition reaction of three alkynes entails two key steps (Scheme 4).[10] First, the oxidative addition that takes place between two of the alkyne ligands initially coordinated to the metal centre. Second, the insertion of the last alkyne already coordinated to the metal to generate a metallacycloheptatriene intermediate in a Schore's mechanism.[11] Depending on the catalysts used, type of unsaturations, and experimental conditions, this second key step can also proceed via a metal-mediated [4+2] cycloaddition to yield a metallanorbornadiene intermediate or a [2+2] cycloaddition to give a metallabicyclo[3.2.0]heptatriene. In a subsequent step, the intermediate formed suffers a ring closure through a reductive elimination process. Finally, the catalytic cycle is completed with the recovery of the catalyst and release of the product.

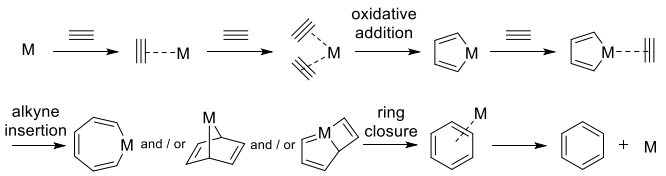

Scheme 4. Generally accepted mechanism for the [2+2+2] cycloaddition reaction involving three alkynes (M = transition metal complex).

For those [2+2+2] cycloaddition reactions in which unsaturations other than alkynes participate, the same general mechanism is postulated to take place but with some particularities. In our specific case, it was necessary to determine the order in which the unsaturations participate in the catalytic cycle (i.e., whether the oxidative addition occurs between the alkyne and the alkene, between the alkyne and the allene, or between the alkene and the allene). Moreover, it is important to discuss the diastereoselectivity experimentally found when C*sp*^{2}-containing unsaturations are involved. In order to shed more light on which catalytic species participated in each of the processes catalysed by $[RhCl(PPh_3)_3]$ and $[RhCl(CO)_2]_2$, we undertook several empirical tests intended to determine the ligands present in the rhodium coordination sphere.

Let us start with the mechanism for the cyclization catalysed by $[RhCl(PPh_3)_3]$. Active species in the cycloaddition reaction catalysed by Wilkinson's catalyst are generated after PPh_3 release. In order to determine how many PPh_3 units are coordinated to the Rh centre in the catalytically relevant species, we took advantage of the presence of phosphorus atoms in Wilkinson's catalyst to monitor and detect these species by NMR spectroscopy. When either catalytic or stoichiometric mixture of substrate **3a** and Wilkinson's catalyst in toluene-D_8 was introduced to the NMR spectrometer and analysed at room temperature in a sealed NMR tube, the formation of two new products (in a 1:0.8 ratio) was observed both by ^{1}H and ^{31}P{^{1}H} NMR spectroscopy (see Figure 2a and the SI for full experimental details and spectra). Each species gave a doublet in the ^{31}P NMR spectra, at 31.93 ppm ($^1J_{P\text{-}Rh}$ = 126.6 Hz) and 33.40 ppm ($^1J_{P\text{-}Rh}$ = 127.0 Hz), respectively. We postulated that they corresponded to coordination species containing only one triphenylphosphine ligand and carried out 2D NMR experiments such as ^{1}H-^{1}H COSY, DOSY and ^{1}H-^{31}P HMBC to fully characterize them. Key to the assignment was the analysis of the ^{1}H-^{31}P HMBC, which showed cross-peaks between the P and both the terminal alkyne and the allenic protons in the two species (see Spectra SII-5 in the SI), allowing us to conclude that both species correspond to rhodium complexes containing one triphenylphosphine ligand coordinated to the alkyne and the tw double bonds of the allene moieties of the substrate.

In order to shed more light on their identity, B3LYP-D3/cc pVDZ-PP calculations were undertaken to find the most stabl coordination species including one PPh_3 unit. As a result of these we were able to establish the relative stability order of th coordinated species (Scheme 5). The two lowest-in-energy specie (**A0a** and **A0b**) consist of two compounds in which the rhodium i coordinated to the alkyne and to the distal double bond of the allene These two new coordinations replace two of the triphenylphosphin ligands of the initial Wilkinson catalyst. Attempts to optimiz complexes in which the allene was coordinated with the interna double bond invariably led to the isomerization of coordination t the distal double bond. The two species differ in the relativ orientation of the ligands in the square-planar coordination sphere c the coordination compound (Figure 3). The next two species **A0** and **A0d** are located at 2.0 and 5.4 kcal mol^{-1} higher in energ respectively, compared to the lowest in energy **A0a** species. Thes geometries consist of the coordination of the alkyne and alken motifs to the rhodium centre and are differentiated by the opposit configuration of the alkene.

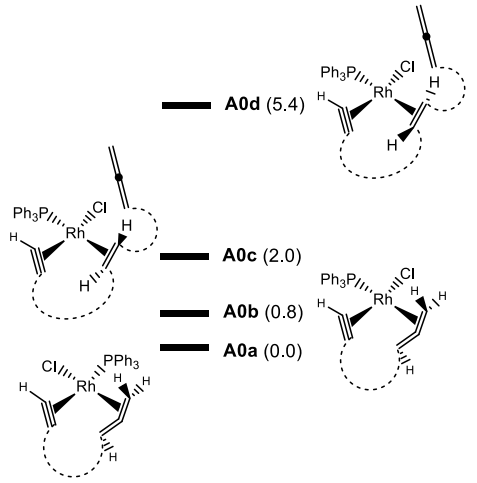

Scheme 5. Most stable coordination intermediates computed by DFT calculations. Energies in kcal mol^{-1}.

Taking the experimental and computational data together, **A0a** and **A0b** were assigned as the two species that are experimentally detected. The calculated small energy difference of 0.8 kcal mol^{-1} between **A0a** and **A0b** concurs with the similar amounts of these compounds that are detected experimentally. Furthermore, analysis of the NOESY spectra showed exchange cross-peaks indicating that

10.1002/chem.201703194

these species are in slow equilibrium in the NMR time scale (see the SI for spectra and equilibrium scheme).

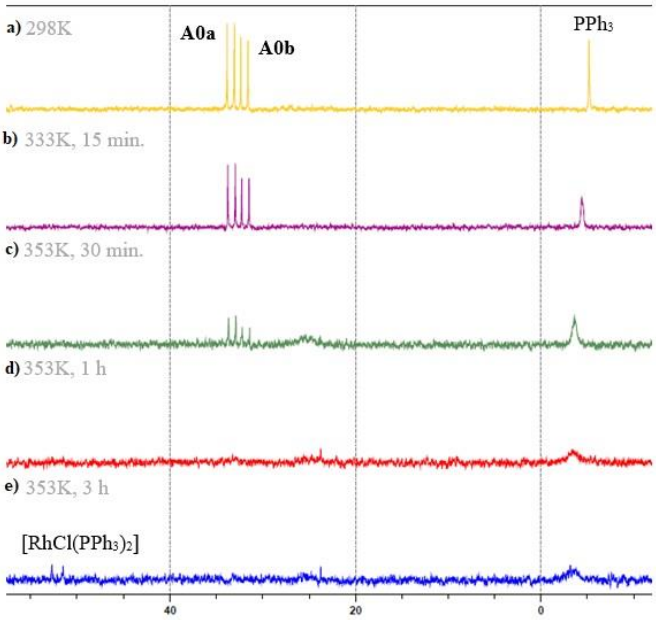

Figure 2. $^{31}P\{^{1}H\}$ NMR monitoring of the [2+2+2] cycloaddition reaction of **3a** using catalytic system A.

The sample was then heated inside the NMR spectrometer to 353K and periodically monitored by ^{1}H and $^{31}P\{^{1}H\}$ NMR spectroscopy (Figure 2). No change was observed from 298K to 333K, but when the reaction was gradually heated to 353K, the two doublets corresponding to **A0a** and **A0b** started to vanish, the PPh_3 signal broadened and no clear signal appeared. Our interpretation of these results is that the catalytically active species might not have coordinated phosphine and that $[RhCl(PPh_3)_2]$, which is detected in the reaction media towards the end of the reaction, acts as a resting state for the rhodium.

Based on the precedents in our research group[10d] and the results of the NMR study, we decided to analyse catalytically active species containing one or no triphenylphosphine ligands coordinated to the rhodium centre. In Scheme 6, the Gibbs energy profiles of the most favourable pathways leading to *syn*-**4a** and *anti*-**4a** from **3a** under $[RhCl(PPh_3)_3]$ catalysis are depicted. Oxidative addition from either **A0a** or **A0b** would lead to a cycloadduct that is regioisomeric to the ones that were isolated and, therefore, direct oxidative addition was not considered from these experimentally detected intermediates. Oxidative addition from either **A0c** or **A0d** was evaluated but high energy barriers ($\Delta G^{\ddagger}$ = 49.2 kcal mol^{-1} and $\Delta G^{\ddagger}$ = 39.7 kcal mol^{-1}, respectively) were found and so these pathways were ruled out. Instead, the endergonic loss of the PPh_3 ligand from **A0a** and **A0b** was considered to generate **A1**, from which a somewhat lower barrier for the oxidative addition was calculated to be 37.2 kcal mol^{-1}.

Although **A1** has a lower energy barrier in the oxidative addition than **A0d**, the barrier obtained is still too high to explain experimental outcome. However, a lower energy pathway for the oxidative addition was found by the coordination of the allene moiety to the metal centre to yield **A2a** or **A2b**. The main difference between **A2a** and **A2b** is the orientation of the allene group that is *ca*. perpendicular to the Rh–Cl bond in **A2a** and parallel in **A2b** (see Figure 4). As expected from the molecular orbitals of a d^8 ML_4 fragment,[12] these two orientations lead to complexes with a small energy difference. The different orientation of the allene fragment is important because it places the H atom of the internal allene in the right position to provide *syn*-**4a** (**A2a**) or *anti*-**4a** (**A2b**) products. Oxidative addition from **A2a** through **TS(A2a,A3a)** and from **A2b** via **TS(A2b,A3b)** have Gibbs energy barriers of 30.6 kcal mol^{-1} and 31.7 kcal mol^{-1}, respectively. The two oxidative addition processes leading to **A3a** and **A3b** are exergonic by 1.0 kcal mol^{-1} and endergonic by 3.1 kcal mol^{-1}, respectively.

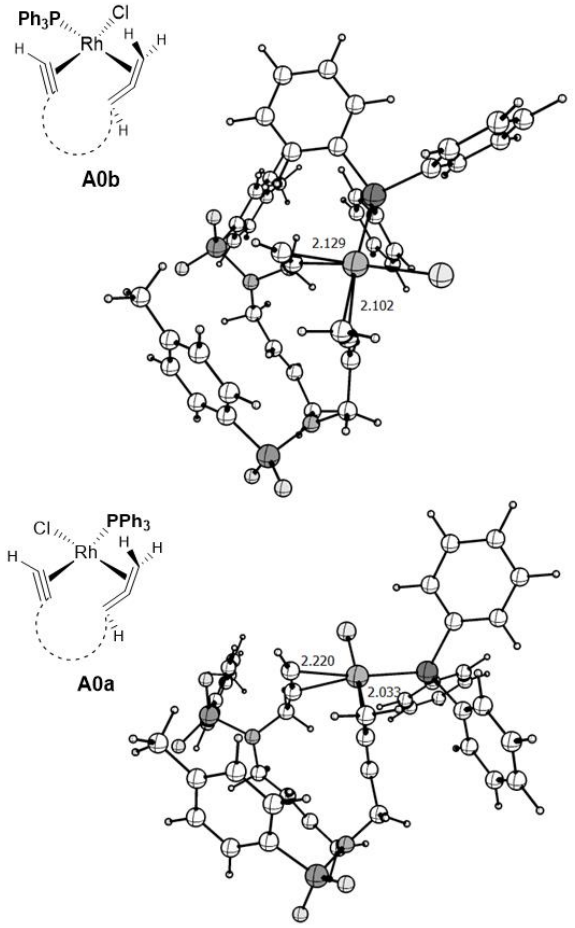

Figure 3. Coordination compounds **A0a** and **A0b** observed by NMR experiments whe **3a** was mixed with stoichiometric amounts of Wilkinson's catalyst. Geometries fro B3LYP-D3/cc-pVDZ-PP optimizations. Distances are given in Å.

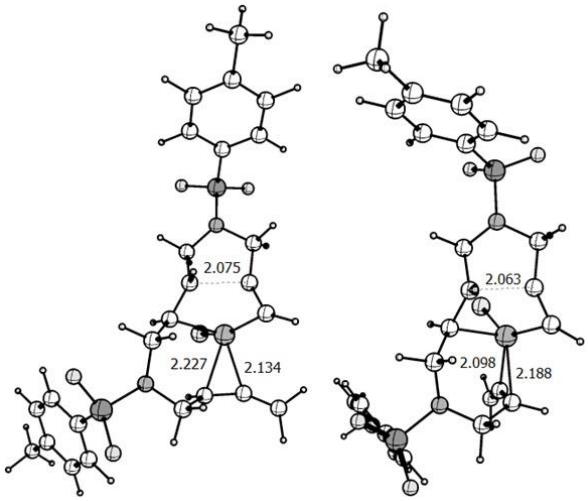

Figure 4. Optimized structures (B3LYP-D3/cc-pVDZ-PP) for **TS(A2a,A3a)** (left) and **TS(A2b,A3b)** (right). Relevant distances are given in Å.

10.1002/chem.201703194

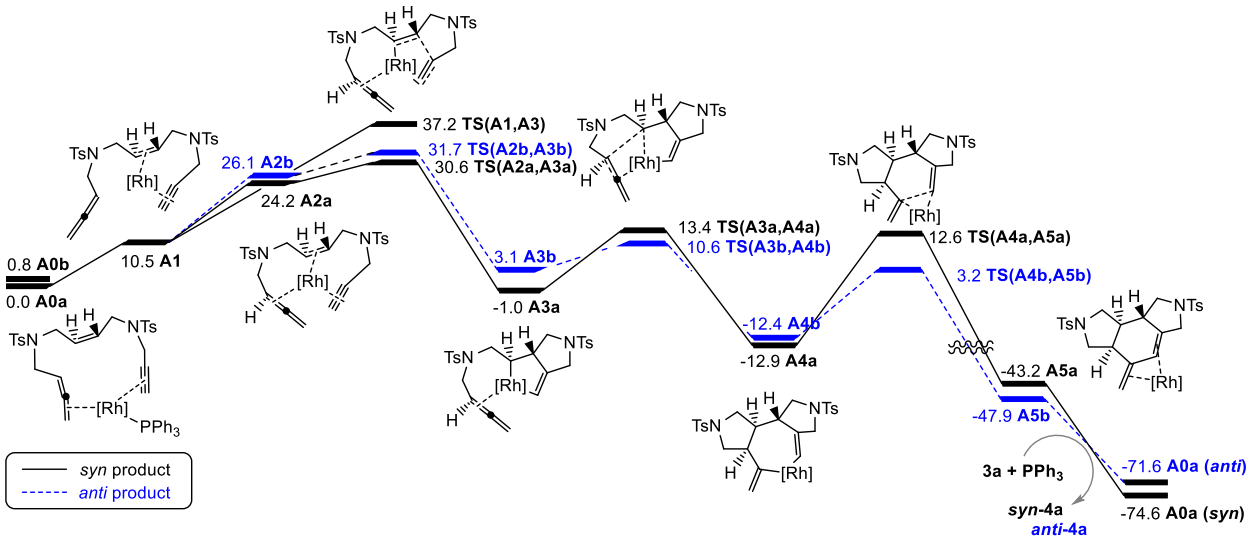

Scheme 6. Gibbs energy profile (kcal mol^{-1}) for the most favorable route of the [RhCl(PPh$_3$)$_3$]-catalysed [2+2+2] cycloaddition of allene-ene-yne **3a** leading to *syn*-**4a** and *anti*-**4** Energies are relative to complex **A0a**. Only the schematic drawings of the structures for the *syn* path are depicted. [Rh] = RhCl.

We then proceeded to evaluate the insertion step. From intermediates **A3a** and **A3b**, several possibilities emerge for the insertion of the internal double bond of the allene group. Attacks leading to rhodacycloheptene were computed for the insertion of the allene into a Rh-C(sp^3) or Rh-C(sp^2) bonds. Moreover, a rhodanorbornane intermediate could also be generated through a Diels-Alder-like TS. However, despite many attempts, we were unable to locate either the TS or the rhodanorbornane intermediate for the Diels-Alder-like attack. By comparing the energy barriers for the remaining cases, we observed a clear preference for the insertion taking place on the Rh-C(sp^3) bond. **TS(A3a,A4a)** and **TS(A3b,A4b)** shown in Figure 5 had the two lowest energy barriers with $\Delta G^{\ddagger}$ = 14.4 kcal mol^{-1} and $\Delta G^{\ddagger}$ = 7.5 kcal mol^{-1}, respectively.

The following step is the reductive elimination and involves the formation of the C-C bond that affords the final cyclohexene ring η^4-coordinated to RhCl. The energy barriers found for such process were computed to be $\Delta G^{\ddagger}$ = 25.5 kcal mol^{-1} and $\Delta G^{\ddagger}$ = 15.6 kcal mol^{-1} for **TS(A4a,A5a)** and **TS(A4b,A5b)**, respectively. In both pathways, the highest energy barriers are associated to the oxidative addition step and so the rate-determining step for this route resides at the beginning of the process.

The overall reaction is exergonic by 71.6-74.6 kcal mol^{-1} and the energy span between the turnover frequency (TOF) determining intermediate (TDI) and TOF determining TS (TDTS)[13] is 30.6 kcal mol^{-1} and 31.7 kcal mol^{-1} for pathways leading to *syn*-**4a** and *anti*-**4a**, respectively.

Further support for the mechanism being comprised of phosphine-free intermediates was gained by running the cycloaddition reaction using [RhCl(ethylene)$_2$]$_2$ as a catalyst. *syn*-**4a** and *anti*-**4a** were obtained in a 41% yield (2.5 : 7.5 d.r.) after heating a solution of **3a** in toluene to 100ºC for 1h with this catalyst. This result indicated that the reaction can take place in the absence of PPh$_3$ ligands and probably through the same catalytic intermediates, since the ethylene ligand can easily be released due to its lability when the substrate enters the coordination sphere of the rhodium centre.

We then turned our attention to the [RhCl(CO)$_2$]$_2$ catalyst, which was observed to afford the opposite diastereoisomeric ratio when **3a** is employed. Once again, the study was begun by running an empirical test to obtain more information about the coordination sphere of the metal centre. In the case of the [RhCl(CO)$_2$]$_2$, we decided to use electrospray ionization mass spectrometry (ESI-MS) in order to propose a structure for the catalytically active species.[1
With this aim, we set up the reactions that afford **4a** and **4d** unde
the optimized conditions and several aliquots were sequentiall
taken from the reaction crude and analysed by ESI-MS. After som
optimization, we found that best sensitivity was obtained by mixin
the aliquots taken from the reactions with a solution of LiCl 0.01M
in methanol prior to injection and analysis in the negative io
mode.[15] When **3a** was employed, two peaks at *m/z* = 684.8 and *m*
= 656.9 were detected, which were assigned to [RhCl(**3a**)(CO)
Cl]$^-$ and [RhCl(**3a**) + Cl]$^-$. Analogously, when **3d** was used, peak
were observed at *m/z* = 726.9 ([RhCl(**3d**)(CO) + Cl]$^-$) and *m/z*
698.8 ([RhCl(**3b**) + Cl]$^-$). Furthermore, CID fragmentation o
[RhCl(**3a**)(CO) + Cl]$^-$ or [RhCl(**3d**)(CO) + Cl]$^-$ showed th
formation of a peak at [M-28]$^-$ corresponding to the loss of the C
group to give [RhCl(**3a**) + Cl]$^-$ or [RhCl(**3d**) + Cl]$^-$, respectively.
seems from these results that at least one carbon monoxide may b
present in the catalytically active species.

At this point we performed a similar computational analysis of th
different possible pathways that could lead to the observe
compounds. Taking into account the precedents found in th
literature[16] and the ESI-MS results, we considered the monomeri
form of the catalyst, i.e., RhCl(CO)$_2$. The analysis began b
analysing the different possibilities regarding the coordination of th
allene, alkene, and alkyne moieties to the rhodium centre. I
addition to this, we also computed the different intermediates an
TSs that can intervene, depending on the number of carbony
ligands involved: none, one or two.

The proposed mechanism (Scheme 7) starts with the coordination o
the alkyne and alkene unsaturations to the rhodium centre with tw
carbonyl ligands and the chloride (**B1**). From this point onwards, th
intermediate can afford the rhodacyclopentene intermediate **B**
surmounting an energy barrier of $\Delta G^{\ddagger}$ = 15.1 kcal mol^{-1} for this
oxidative addition process. As in the previous case, the oxidative
addition between the alkene and the alkyne was the most favourable.
Even though **B2**, which could be obtained from **B1** after releasing a
CO ligand, is a more stable intermediate by 8.1 kcal mol^{-1}, we
computed that the corresponding **TS(B2,B3')** is located at $\Delta G^{\ddagger}$ =
26.8 kcal mol^{-1}, allowing this alternative path to be discarded. This
is not an unexpected result given the higher σ-donation than π-
backdonation of the CO ligand.[17] Thus, the presence of CO favours
the oxidation of Rh(I) to Rh(III) and the barrier of the oxidative
addition step is lower when catalysed by RhCl(CO)$_2$ than by
RhCl(CO).

10.1002/chem.201703194

Having reached rhodacyclopentene intermediate **B3**, this intermediate rearranges to **B4a** or **B4b**, in which the allene moiety coordinates to the rhodium centre, giving rise to the two possible orientations of the protons for the generation of the *syn* and *anti* diastereoisomers. For the synthesis of the *anti* cycloadduct, loss of a CO ligand in **B4b** occurs, releasing 2.8 kcal mol^{-1} to yield **B5b**. From **B5b**, insertion of the internal double bond of the allene into the Rh-C(sp^3) bond generates rhodacycloheptene intermediate **B7b** with an *anti* C-C fusion in a process with a 14.8 kcal mol^{-1} barrier (Figure 5). On the other hand, **B4a** evolves to the cycloadduct with the *syn* C-C fusion, through a pathway that differs from the previous one in two aspects. Firstly, there is no CO dissociation, and, secondly, the insertion of the allene takes place on the Rh-C(sp^2) bond of **B4a**. The energy barrier for the formation of **B6a** is only 1.4 kcal mol^{-1}.

The ring closure in **B7b** towards the *anti* diastereoisomer was computed to be possible by passing over an energy barrier of 11.0 kcal mol^{-1} to give **B8b**. In the pathway leading to the *syn* diastereoisomer we observed that the stability of **B6a** significantly increased by 9.6 kcal mol^{-1} when the two carbonyl ligands were lost to yield **B7a**. However, looking at the final step, the ring closure process was observed to be more favourable if the carbonyl ligand was recovered, since **TS(B6a,B8a)** was located at $\Delta G^{\ddagger}$ = 16.2 kcal mol^{-1} with respect to the most stable intermediate **B7b**, which is a much more plausible value than the corresponding reductive elimination via **TS(B7a,B8a')**, $\Delta G^{\ddagger}$ = 40.4 kcal mol^{-1}.

Overall, the catalytic cycle showed itself to be exergonic by 71.6-74.6 kcal mol^{-1} and the energetic difference between TDI and TDTS was 15.1 kcal mol^{-1} (oxidative addition) for the *anti* pathway, and 16.2 kcal mol^{-1} (ring closure) for the *syn* pathway. The generation of the two diastereoisomers that have been experimentally detected could be justified by looking at the low energy span differences (1.1 kcal mol^{-1}) of the rate-determining steps between the pathways leading to *syn*-**4a** and *anti*-**4a**, in favour of the *anti* diastereoisomer, which matches the empirical results. The results of the empirical tests carried out using ESI-MS to detect reaction intermediates support the type of intermediates proposed for this catalytic cycle. We were able to observe peaks corresponding to [RhCl(**3**)(CO)] species, which corroborate the coordination sphere of the intermediates depicted in Scheme 7.

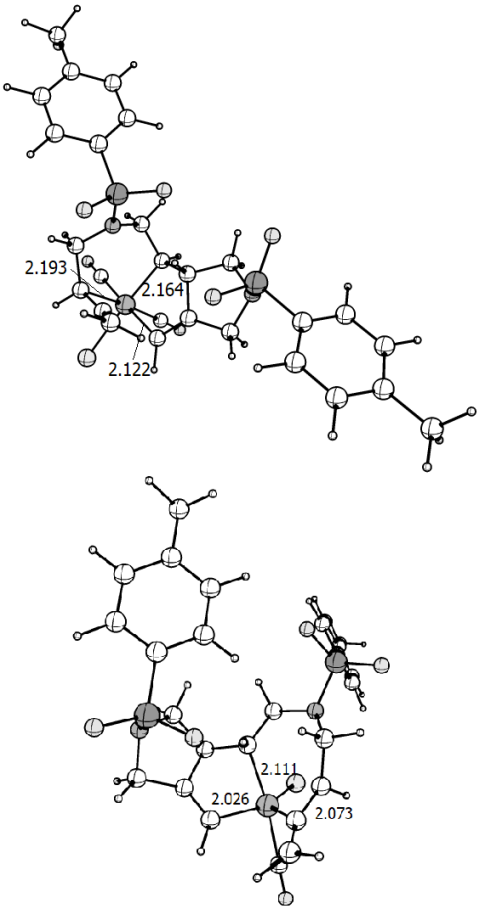

Figure 5. Optimized structures (B3LYP-D3/cc-pVDZ-PP) for **TS(B4a,B6a)** (top) ar **TS(B5b,B7b)** (bottom). Most relevant distances given in Å.

Comparison of the two proposed catalytic cycles allowed us t explain computationally the experimental detection of tw diastereoisomers, since very low energetic differences were foun between similar potential energy surfaces leading to the *syn* and th *anti* diastereoisomers. Furthermore, the difference in selectivity o the two catalytic systems can be attributed to the variation in th coordination sphere of the catalytically-active species: th [RhCl(PPh_3)$_3$] catalyst cycle runs on a catalytic species with only chloride ligand, while the outcome for the [RhCl(CO)$_2$]$_2$ catalys relies on the number of carbonyl units coordinated to the metalli centre. On the other hand, the need to heat the system to 100 °C when [RhCl(PPh_3)$_3$] catalyst is employed and to just 60 °C whe [RhCl(CO)$_2$]$_2$ is used is in accordance with the energy barriers foun since the first requires about 30 kcal mol^{-1} to complete the cycle an only ca. 15 kcal mol^{-1} for the second.

10.1002/chem.201703194

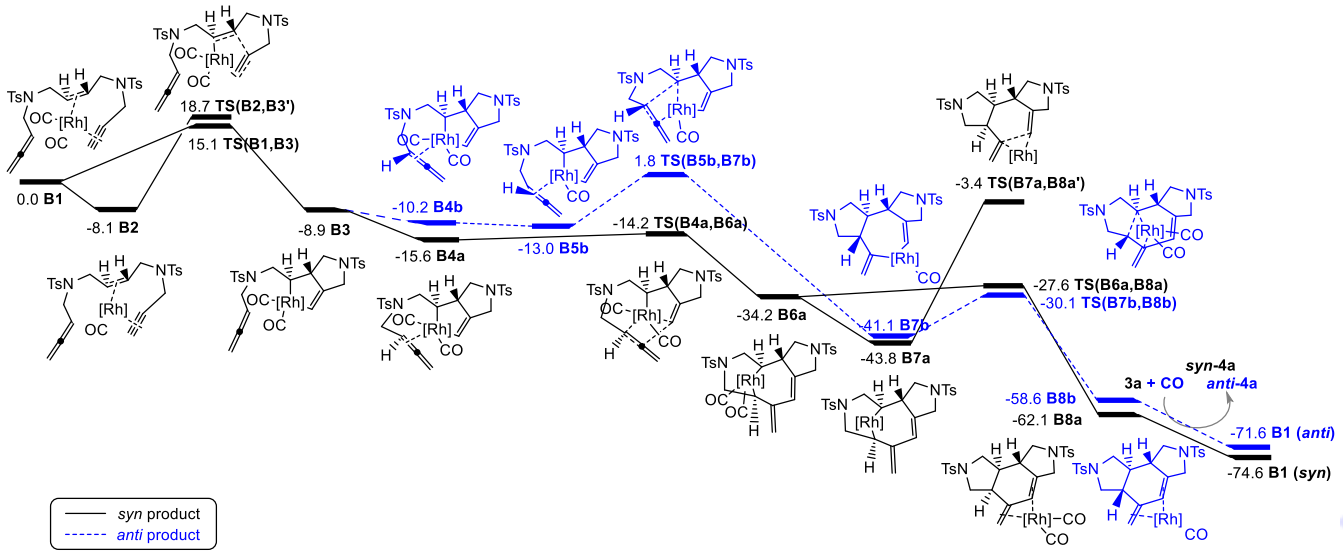

Scheme 7. Gibbs energy profile (kcal mol^{-1}) for the most favourable routes of the [RhCl(CO)$_2$]-catalyzed [2+2+2] cycloaddition of allene-ene-yne **3a** leading to *syn*-**4a** and *anti*-**4** In this Scheme [Rh] = RhCl. Schematic drawings of the structures for the *syn* path in black and for the *anti* path in blue.

Conclusion

The reactivity of linear allene-(*E*)-ene-yne substrates bearing an *N*-tosyl tether was evaluated in the rhodium-catalysed [2+2+2] cycloaddition reaction. Three catalytic systems were tested: the neutral Wilkinson complex, the cationic [Rh(cod)$_2$]BF$_4$ in combination with a biphosphine ligand, and the dimeric complex [RhCl(CO)$_2$]$_2$. All three catalysts were able to promote the cycloaddition regioselectively involving the internal double bonds of the allene allowing for the preparation of scaffolds featuring exocyclic dienes. However, the diastereoselectivity of the process seems to be catalyst-dependent. Regarding the mechanism operating in these transformations, it is important to highlight that oxidative addition always takes place between the alkyne and the alkene and that the diastereoselectivity is defined later during the allene insertion step. Allene inserts with the inner double bond preferentially the Rh–C$_{sp3}$ bond. The variable and low diastereoselectivity of the process can be ascribed to the small differences in the rate-determining energy barriers.

Experimental Section

Unless otherwise noted, materials were obtained from commercial suppliers and used without further purification. All reactions requiring anhydrous conditions were conducted in oven-dried glassware under a dry nitrogen atmosphere. The solvents were removed under reduced pressure with a rotary evaporator. Residues were purified by chromatography on a silica gel column (230–400 mesh) by using mixtures of hexane/ethyl acetate as the eluent.

^{1}H and ^{13}C NMR spectra were measured on a 400 or a 300 MHz NMR spectrometer. ^{1}H and ^{13}C chemical shifts (δ) are referenced to internal solvent resonances and reported relative to SiMe$_4$. The chemical shifts were assigned on the basis of 2D COSY, NOESY, DOSY, ^{1}H-^{13}C HSQC, ^{1}H-^{13}C HMBC and ^{1}H-^{31}P HMBC experiments performed under routine conditions. Electrospray mass spectrometry analyses were recorded on an Esquire 6000 ion trap mass spectrometer (Bruker) equipped with an electrospray ion source, operated in positive ESI(+) ion mode. IR spectra were recorded with an FT-IR using a single reflection ATR system as a sampling accessory.

Rh(I)-catalyzed [2+2+2] cycloaddition reaction of allene-ene-yne derivative 3a. General procedure using catalytic system A (Entry 1, Table 1): In a 10 mL two-necked round-bottom flask, a mixture of **3a** (24.6 mg, 0.050 mmol) and tris(triphenylphospine)rhodium(I) chloride (5.6 mg, 0.006 mmol, 10 mol %) was dissolved in anhydrous toluene (3 mL) and heated to 100ºC. The mixture was stirred for 5h until completion (TLC monitoring). The solvent was removed under reduced pressure and the reaction crude was purified by column chromatography on silica gel using a mixture of hexanes/ethyl acetate (8:2) as the eluent to afford **4a** (13.8 mg, 56% yield) as a colourless solid.

General procedure using catalytic system B (Entry 6, Table 1): In a 10 mL two-necked round-bottom flask, a mixture of bis(1,5-cyclooctadiene)rhodium(I) tetrafluoroborate (2.1 mg, 0.0052 mmol, 10 mol %) and (*R*)-DTBM-SegPhos (6.6 mg, 0.0056 mmol) was dissolved in anhydrous dichloromethane (3 mL) and hydrogenated for 30 min. The solvent was then removed under vacuum, anhydrous dichloroethane (3 mL) was introduced, and the reaction mixture was heated to 60 °C. Allene-ene-yne **3** (25.4 mg, 0.052 mmol) was slowly added to the previous mixture. The mixture was stirred for 5h until completion (TLC monitoring). The solvent was removed under reduced pressure and the reaction crude was purified by column chromatography on silica gel using a mixture of hexanes/EtOAc (8:2) as the eluent to afford **4a** (7.8 mg, 31% yield) as a colourless solid.

General procedure using catalytic system C (Entry 9, Table 1): In a 10 mL two-necked round-bottom flask, **3a** (24.2 mg, 0.050 mmol) was dissolved in anhydrous toluene (3 mL) and heated to 60 ºC. Di-μ-chloro-tetracarbonyldirhodium(I) (2.37 mg, 0.006 mmol, 10 mol %) was slowly added to the previous solution. The mixture was stirred for 20 min. until completion (TLC monitoring). The solvent was removed under reduced pressure and the reaction crude was purified by column chromatography on silica gel using a mixture of hexane/EtOAc (8:2) as the eluent to afford **4a** (11.8 mg, 49% yield) as a colourless solid.

Cycloadduct 4a was obtained as an inseparable mixture of the two diastereoisomers *syn* and *anti*. ^{1}H-NMR (500 MHz, CDCl$_3$, TMS): δ(ppm) 1.48 (m, 1H$_{anti}$), 1.74 (m, 1H$_{syn}$), 1.84 (m, 1H$_{syn}$), 2.34 (m, 1H$_{anti}$), 2.43 (m, 1H$_{syn}$), 2.46 (s, 3H$_{syn}$ + 3H$_{anti}$), 2.46 (m, 2H$_{anti}$), 2.51 (s, 3H$_{syn}$ + 3H$_{anti}$), 2.83 (dd, $^2J_{H,H}$ = 11.5 Hz, $^3J_{H,H}$ = 8.8 Hz, 1H$_{syn}$), 2.90 (m, 1H$_{syn}$), 2.97 (m, 1H$_{anti}$), 3.14 (dd, $^2J_{H,H}$ = $^3J_{H,H}$ = 10.5 Hz, 1H$_{anti}$), 3.30 (d, $^2J_{H,H}$ = 10.5 Hz, 1H$_{syn}$), 3.39 (dd, $^2J_{H,H}$ = 10.5 Hz, $^3J_{H,H}$ = 4.5 Hz, 1H$_{syn}$), 3.55 (m, 1H$_{syn}$), 3.60-3.66 (m, 2H$_{syn}$ + 1H$_{anti}$), 3.69 (d, $^2J_{H,H}$ = 15.0 Hz, 1H$_{anti}$), 3.76-3.84 (m, 2H$_{anti}$), 4.01 (d, $^2J_{H,H}$ = 15.0 Hz, 1H$_{syn}$), 4.10 (d, $^2J_{H,H}$ = 15.0 Hz, 1H$_{syn}$), 4.68 (s, 1H$_{anti}$), 4.88 (s, 1H$_{anti}$), 4.91 (s, 1H$_{syn}$), 4.97 (s, 1H$_{syn}$), 5.93 (s, 1H$_{syn}$), 5.98 (s, 1H$_{anti}$), 7.35 (d, $^3J_{H,H}$ = 8.0 Hz, 2H$_{syn}$ + 2H$_{anti}$), 7.40 (d, $^3J_{H,H}$ = 8.0 Hz, 2H$_{syn}$ + 2H$_{anti}$), 7.69 (d, $^3J_{H,H}$ = 8.0 Hz, 2H$_{syn}$ + 2H$_{anti}$), 7.74 (d, $^3J_{H,H}$ = 8.0 Hz, 2H$_{syn}$ + 2H$_{anti}$); ^{13}C-NMR (75 MHz, CDCl$_3$, TMS, *syn*): δ(ppm) 21.6, 29.7, 38.3, 39.9, 42.2, 50.8, 51.0, 52.5, 52.9, 115.2, 120.6, 127.1, 127.6, 129.9, 138.0, 138.7, 143.9, 144.3; HRMS calcd. For [C$_{25}$H$_{28}$N$_2$O$_4$S$_2$ + Na] 507.1388. Found: 507.1388.

Cycloadduct 4b: was obtained as pure *syn* diastereoisomer. IR(ATR): *ν* (cm^{-1}) 2924, 1334, 1153; ^{1}H-NMR (400 MHz, CDCl$_3$, TMS): δ(ppm) 1.63 (br, 3H), 1.73 (m, 1H), 1.81 (m, 1H), 2.35 (dd, $^2J_{H,H}$ = 10.4 Hz, $^3J_{H,H}$ = 8.6 Hz, 1H), 2.44 (s, 3H), 2.49 (s, 3H), 2.81 (dd, $^2J_{H,H}$ = 11.6 Hz, $^3J_{H,H}$ = 9.6 Hz, 1H), 2.94 (s, 1H), 3.23 (d, $^2J_{H,H}$ = 10.4 Hz, 1H), 3.38 (dd, $^2J_{H,H}$ = 10.4 Hz, $^3J_{H,H}$ = 4.8 Hz, 1H), 3.52-3.62 (m, 3H), 3.98 (d, $^2J_{H,H}$ = 15.2 Hz, 1H), 4.85 (s, 1H), 5.06 (s, 1H), 7.33 (d, $^3J_{H,H}$ = 8.4 Hz, 2H), 7.38 (d, $^3J_{H,H}$ = 8.4 Hz, 2H), 7.68 (d, $^3J_{H,H}$ = 8.4 Hz, 2H), 7.72 (d, $^3J_{H,H}$ = 8.4 Hz, 2H); ^{13}C-NMR (100 MHz, CDCl$_3$, TMS): δ(ppm) 21.6, 30.9, 38.3, 40.0, 42.2, 50.8, 51.0, 52.5, 53.0, 115.2, 120.6, 127.1, 127.6, 129.8, 129.9, 138.1, 138.8, 144.2, HRMS calcd. For [C$_{26}$H$_{30}$N$_2$O$_4$S$_2$ + Na]$^+$: 521.1539. Found: 521.1548.

Cycloadduct 4c: was obtained as pure *syn* diastereoisomer. IR(ATR): *ν* (cm^{-1}) 2925, 1339, 1155; ^{1}H-NMR (400 MHz, CDCl$_3$, TMS): δ(ppm) 0.91 (t, $^3J_{H,H}$ = 7.6 Hz, 3H), 1.79-1.82 (m, 2H), 2.06 (q, $^3J_{H,H}$ = 7.6 Hz, 2H), 2.36 (m, 1H), 2.44 (s, 3H), 2.49 (s, 3H), 2.82 (dd, $^2J_{H,H}$ = 11.6 Hz, $^3J_{H,H}$ = 9.6 Hz, 3H), 2.92 (m, 1H), 3.23 (d, $^2J_{H,H}$ = 10.4 Hz,

1H), 3.36 (dd, $^2J_{H,H}$ = 10.4 Hz, $^3J_{H,H}$ = 4.4 Hz, 1H), 3.52-3.63 (m, 3H), 3.98 (m, 1H), 4.87 (s, 1H), 5.10 (s, 1H), 7.34 (d, $^3J_{H,H}$ = 8.4 Hz, 2H), 7.38 (d, $^3J_{H,H}$ = 8.4 Hz, 2H), 7.68 (d, $^3J_{H,H}$ = 8.4 Hz, 2H), 7.72 (d, $^3J_{H,H}$ = 8.4 Hz, 2H); ^{13}C-NMR (100 MHz, $CDCl_3$, TMS): δ(ppm) 13.0, 21.6, 21.8, 29.7, 38.9, 39.8, 43.5, 51.4, 52.5, 53.2, 111.8, 127.1, 127.7, 130.8, 132.6, 133.6, 133.8, 138.3, 143.9, 144.2; HRMS calcd. For $[C_{27}H_{32}N_2O_4S_2 + Na]^+$: 535.1696. Found: 535.1675.

Cycloadduct 4d: was obtained as an inseparable mixture of the two diastereoisomers *syn* and *anti*. ^{1}H-NMR (400 MHz, $CDCl_3$, TMS, ***syn***): δ(ppm) 0.90 (d, $^3J_{H,H}$ = 6.8 Hz, 3H), 0.95 (d, $^3J_{H,H}$ = 6.8 Hz, 3H), 1.63 (m, 1H), 1.75 (m, 1H), 2.35-2.45 (m, 1H + 1H), 2.42 (s, 3H), 2.48 (s, 3H), 2.71 (dd, $^2J_{H,H}$ = 11.6 Hz, $^3J_{H,H}$ = 9.6 Hz, 1H), 2.98 (m, 1H), 3.26 (d, $^2J_{H,H}$ = 10.4 Hz, 1H), 3.38 (dd, $^2J_{H,H}$ = 10.4 Hz, $^3J_{H,H}$ = 4.8 Hz, 1H), 3.54-3.60 (m, 1H + 1H + 1H), 3.95 (m, 1H), 5.19 (d, $^3J_{H,H}$ = 10.4 Hz, 1H), 5.76 (d, $^3J_{H,H}$ = 2.4 Hz, 1H) 7.32 (d, $^3J_{H,H}$ = 8.4 Hz, 2H), 7.38 (d, $^3J_{H,H}$ = 8.4 Hz, 2H), 7.66 (d, $^3J_{H,H}$ = 8.4 Hz, 2H), 7.72 (d, $^3J_{H,H}$ = 8.4 Hz, 2H); ^{13}C-NMR (100 MHz, $CDCl_3$, TMS, ***syn***): δ(ppm) 21.6, 23.0, 23.3, 27.6, 38.1, 38.5, 39.9, 50.0, 50.8, 52.3, 53.2, 122.2, 127.1, 127.6, 128.2, 129.8, 129.9, 132.7, 133.7, 134.5, 140.0, 143.8, 144.3; HRMS calcd. For $[C_{28}H_{34}N_2O_4S_2 + Na]^+$: 549.1858. Found: 549.1855.

Cycloadduct 4e: was obtained as an inseparable mixture of the two diastereoisomers *syn* and *anti*. ^{1}H-NMR (300 MHz, $CDCl_3$, TMS): δ(ppm) 1.28 (m, 1H$_{anti}$), 1.82-1.88 (m, 2H$_{syn}$), 2.38 (m, 1H$_{anti}$), 2.42-2.48 (m, 1H$_{syn}$ + 2H$_{anti}$), 2.44 (s, 3H$_{syn}$ + 3H$_{anti}$), 2.50 (s, 3H$_{syn}$ + 3H$_{anti}$), 2.77-2.94 (m, 2H$_{syn}$ + 1H$_{anti}$), 3.01 (m, 1H$_{anti}$), 3.14 (m, 1H$_{anti}$), 3.27-3.38 (m, 2H$_{syn}$), 3.59-3.78 (m, 3H$_{syn}$ + 4H$_{anti}$), 4.04 (d, $^2J_{H,H}$ = 15.0 Hz, 1H$_{syn}$), 4.13 (d, $^2J_{H,H}$ = 15.3 Hz, 1H$_{anti}$), 5.97 (s, 1H$_{syn}$), 6.03 (s, 1H$_{anti}$), 6.38 (s, 1H$_{syn}$), 6.41 (s, 1H$_{anti}$), 7.13-7.38 (m, 9H$_{syn}$ + 9H$_{anti}$), 7.54-7.75 (m, 4H$_{syn}$ + 4H$_{anti}$); ^{13}C-NMR (75 MHz, $CDCl_3$, TMS): δ(ppm) 21.6, 38.4, 38.7, 40.3, 42.5, 50.7, 51.0, 52.4, 122.8, 125.1, 127.2, 127.5, 127.7, 128.2, 128.6, 128.8, 129.8, 131.3, 132.6, 132.8, 133.4, 134.9, 136.8, 136.9, 143.9, 144.3; HRMS calcd. For $[C_{31}H_{32}N_2O_4S_2 + Na]^+$: 583.1701. Found: 583.1697.

Cycloadduct 4g: was obtained as an inseparable mixture of the two diastereoisomers *syn* and *anti*. ^{1}H-NMR (400 MHz, $CDCl_3$, TMS): δ(ppm) 0.86-0.97 (m, 6H$_{syn}$ + 3H$_{syn}$ + 6H$_{anti}$ + 3H$_{anti}$), 1.47 (m, 1H$_{anti}$), 1.67-1.74 (m, 2H$_{syn}$), 1.90 (m, 1H$_{syn}$), 1.98-2.05 (m, 2H$_{syn}$), 2.07-2.11 (m, 2H$_{anti}$), 2.30 (m, 1H$_{anti}$), 2.35-2.43 (m, 1H$_{syn}$ + 2H$_{anti}$), 2.43 (s, 6H$_{syn}$ + 6H$_{anti}$), 2.70 (dd, $^2J_{H,H}$ = 11.6 Hz, $^3J_{H,H}$ = 10.0 Hz, 1H$_{anti}$), 2.82 (dd, $^2J_{H,H}$ = 10.8 Hz, $^3J_{H,H}$ = 9.6 Hz, 1H$_{syn}$), 3.01 (m, 1H$_{anti}$), 3.01 (m, 1H$_{anti}$), 3.15 (dd, $^2J_{H,H}$ = 10.8 Hz, $^3J_{H,H}$ = 9.2 Hz, 1H$_{syn}$), 3.21 (d, $^3J_{H,H}$ = 10.8 Hz, 1H$_{anti}$), 3.70 (dd, $^2J_{H,H}$ = 10.4 Hz, $^4J_{H,H}$ = 4.4 Hz, 1H$_{syn}$), 3.46 (dd, $^2J_{H,H}$ = 9.2 Hz, $^3J_{H,H}$ = 7.2 Hz, 1H$_{syn}$), 3.51-3.74 (m, 6H$_{syn}$ + 6H$_{anti}$), 3.94-4.12 (m, 1H$_{syn}$ + 1H$_{anti}$), 5.30 (dd, $^2J_{H,H}$ = 10.4 Hz, $^3J_{H,H}$ = 2.4 Hz, 1H$_{syn}$), 5.34 (d, $^2J_{H,H}$ = 10.0 Hz, 1H$_{anti}$), 7.32-7.39 (m, 4H$_{syn}$ + 4H$_{anti}$), 7.68-7.72 (m, 4H$_{syn}$ + 4H$_{anti}$); ^{13}C-NMR (100 MHz, $CDCl_3$, TMS): δ(ppm) 13.3, 21.6, 21.9, 23.1, 23.2, 23.5, 23.9, 27.8, 28.1, 38.4, 38.9, 40.0, 43.2, 43.8, 45.5, 50.3, 50.4, 52.3, 53.5, 126.8, 127.2, 127.4, 127.8, 129.8, 129.9, 130.0, 130.9, 131.3, 132.6, 133.9, 134.6, 143.7, 143.9, 144.0 144.3; HRMS calcd. For $[C_{30}H_{38}N_2O_4S_2 + Na]^+$: 577.2171. Found: 577.2171.

Cycloadduct 4h: was obtained as an inseparable mixture of the two diastereoisomers *syn* and *anti*. ^{1}H-NMR (400 MHz, toluene-D_8, TMS): δ(ppm) 1.53 (m, 1H$_{syn}$), 1.81 (m, 1H$_{anti}$), 1.95-1.99 (m, 2H$_{syn}$ + 2H$_{anti}$), 1.95 (s, 3H$_{syn}$ + 3H$_{anti}$), 2.39 (m, 1H$_{syn}$), 2.63 (dd, $^2J_{H,H}$ = 10.4 Hz, $^3J_{H,H}$ = 9.2 Hz, 1H$_{anti}$), 2.72 (dd, $^2J_{H,H}$ = 10.4 Hz, $^3J_{H,H}$ = 8.0 Hz, 1H$_{anti}$), 2.78-2.82 (m, 1H$_{syn}$ + 1H$_{anti}$), 3.04 (m, 1H$_{syn}$), 3.35 (dd, $^2J_{H,H}$ = 9.2 Hz, $^3J_{H,H}$ = 7.2 Hz, 1H$_{anti}$), 3.50 (t, $^2J_{H,H}$ = 9.5 Hz, 1H$_{anti}$), 3.67-3.78 (m, 1H$_{syn}$ + 3H$_{anti}$), 3.89-3.96 (m, 2H$_{syn}$), 4.08 (d, $^3J_{H,H}$ = 14.8 Hz, 1H$_{anti}$), 4.18 (d, $^3J_{H,H}$ = 14.0 Hz, 1H$_{syn}$), 4.42 (s, 1H$_{syn}$), 4.62 (s, 1H$_{anti}$), 4.74 (s, 1H$_{syn}$), 5.49 (s, 1H$_{anti}$), 6.80 (d, $^3J_{H,H}$ = 8.0 Hz, 2H$_{syn}$), 6.84 (d, $^3J_{H,H}$ = 8.0 Hz, 2H$_{anti}$), 7.64 (d, $^3J_{H,H}$ = 8.0 Hz, 2H$_{syn}$), 7.72 (d, $^3J_{H,H}$ = 8.0 Hz, 2H$_{anti}$); ^{13}C-NMR (100 MHz, toluene-D_8, TMS): δ(ppm) 13.7, 41.4, 42.1, 45.9, 48.9, 50.4, 51.6, 51.9, 60.9, 107.5, 113.1, 115.7, 129.4, 129.5, 130.2, 134.3, 136.0, 142.5, 143.5, 144.5, 144.5; HRMS calcd. For $[C_{18}H_{21}NO_3S + Na]^+$: 354.1140. Found: 354.1134.

Computational details: All geometry optimisations were performed without symmetry constraints using the hybrid DFT B3LYP[18] method with the all-electron cc-pVDZ basis set for P, Cl, O, C, and H[19] and the cc-pVDZ-PP basis set containing an effective core relativistic pseudopotential for Rh.[20] The D3 Grimme energy corrections for dispersion with its original damping function[21] were added in all B3LYP/cc-pVDZ-PP calculations. Analytical Hessians were computed at the B3LYP-D3/cc-pVDZ level of theory to determine the nature of stationary points (one or zero imaginary frequencies for transition states and minima, respectively) and to calculate unscaled zero-point energies (ZPEs) as well as thermal corrections and entropy effects by using the standard statistical-mechanics relationships for an ideal gas.[22] These last two terms were computed at 373.15 K (for the $[RhCl(PPh_3)_3]$ cycle) or 333.15 K (for the $[RhCl(CO)_2]_2$ cycle) and 1 atm to provide the reported relative Gibbs energies. Furthermore, the connectivity between stationary points was established by intrinsic reaction path calculations.[23] All calculations were performed with the Gaussian 09[24] program package. Previous studies found that solvent effects due to toluene in [2+2+2] cycloadditions are minor, likely due to the absence of charged or polarized intermediates and transition states in the reaction mechanism.[10a][25] Because the reactions studied are carried out in toluene solution, solvent effects have not been included in the present calculations.

Supporting Information

Experimental procedures for the synthesis of the substrates and full spectroscopic data for all new compounds and intermediates. Gibbs energy profiles for all possible pathways not included in the main paper. Cartesian coordinates of all reactants, intermediates, transition states, and products of the reaction.

Acknowledgements

Financial support from the Spanish Ministry of Education and Science (MINECO) (Project No. CTQ2014-54306-P and CTQ2015-64436-P), the DIUE of the Generalitat de Catalunya (Project No.: 2014SGR931, pre-doctoral grant to D.C. and ICREA Academia 2014 prize to MS), and the FEDER fund (European Fund for Regional Development) for grant UNGI08-4E-801 is gratefully acknowledged. The excellent service by the Centre de Serveis Científics i Acadèmics de Catalunya (CESCA) is gratefully acknowledged. We want to thank Dr. Ana Caballero and Prof. Pedro J. Pérez for helpful discussion.

Abstract in Catalan: S'han preparat satisfactòriament una sèri de substrats de cadena oberta contenint un al.lè, un doble enllaç i u alquí **3a-3h** i s'ha evaluat la seva reacció de cicloaddició [2+2+2 catalitzada per rodi. La cicloaddició és quimioselectiva degut a qu només el doble enllaç intern de l'al.lè reacciona per donar u sistema tricíclic fusionat amb un doble enllaç exocíclic L'estereoselectivitat del procés depen del sistema catalític emprat La diferent reactivitat entre l'al.lè, l'alquè i l'alquí s'ha estudiat pe primer cop mitjançant càlculs teòrics basats en la teoria de funcional de la densitat. Aquest estudi mecanístic determina l'ordr en què les insaturacions participen en el cicle catalític.

[1] For selected and recent reviews, see: a) A. Thakur, J. Louie, *Acc. Chem. Res.* **2015**, *48*, 2354; b) M. Amatore, C. Aubert, *Eur. J. Org. Chem.* **2015**, 265; c) Y. Satoh, Y. Obora, *Y. Eur. J. Org. Chem.* **2015**, 5041; d) D. L. J. Broere, R. Ruijter, *Synthesis* **2012**, 2639; e) S. Okamoto, *Heterocycles* **2012**, *85*, 1579; f) Y. Shibata, K. Tanaka, *Synthesis* **2012**, 323; g) N. Weding, M. Hapke, *Chem. Soc. Rev.* **2011**, *15*, 4525; h) R. Hua, M. V. A. Abrenica, P. Wang, *Curr. Org. Chem.* **2011**, *15*, 712; i) M. R. Shaaban, R. El-Sayed, A. H. M. Elwahy, *Tetrahedron* **2011**, *67*, 6095; j) G. Domínguez, J. Pérez-Castells, *Chem. Soc. Rev.* **2011**, *40*, 3430; k) A. Pla-Quintana, A. Roglans, *Molecules* **2010**, *15*, 9230; For a monography, see: l) *Transition-metal-mediated aromatic ring construction* (Ed.: K. Tanaka), Wiley: Hoboken, **2013**.

[2] For selected reviews on the use of allenes in organic synthesis, see: a) S. Yu, S. Ma, *Angew. Chem. Int. Ed.* **2012**, *51*, 3074; *Angew. Chem.* **2012**, *124*, 3128; b) M.A. Tius, *Science of Synthesis*, Thieme, Stuttgart, **2007**, *44*, 353; c) S. Ma, *Chem. Rev.* **2005**, *105*, 2829; d) *Modern Allene Chemistry*, ed. N. Krause, A.S.K. Hashmi, Wiley-VCH, Weinheim, 2004.

[3] For selected reviews on the use of allenes as substrates in cycloaddition and cycloisomerisation reactions, see: a) J. Ye, S. Ma, *Acc. Chem. Res.* **2014**, *47*, 989; b) M. E. Muratore, A. Homs, C. Obradors, A. M. Echevarren, *Chem. Asian J.* **2014**, *9*, 3066; c) B. Alcaide, P. Almendros, C. Aragoncillo, *Chem. Soc. Rev.* **2014**, *43*, 3106; d) C. Aubert, L. Fensterbak, P. Garcia, M. Malacria, A. Simonneau, *Chem. Rev.* **2011**, *111*, 1954; e) F. López, J. L. Mascareñas, *Chem. Eur. J.* **2011**, *17*, 418.

[4] A. Lledó, A. Pla-Quintana, A. Roglans, *Chem. Soc. Rev.* **2016**, *45*, 2003.

[5] a) E. Haraburda, Ò. Torres, T, Parella, M. Solà, A. Pla-Quintana, *Chem. Eur. J.* **2014**, *20*, 5034; b) E. Haraburda, M. Fernández, A. Gifreu, J. Garcia, T. Parella, A. Pla-Quintana, A. Roglans, *Adv. Synth. Catal.* **2017**, *359*, 506.

[6] N. Saito, T. Ichimaru, Y. Sato, *Chem. Asian J.* **2012**, *7*, 1521.

[7] Y. Ohta, S. Yasuda, Y. Yokogawa, K. Kurokawa, C. Mukai, *Angew. Chem. Int. Ed.* **2015**, *54*, 1240.

[8] a) A. Torrent, I. González, A. Pla-Quintana, A. Roglans, M. Moreno-Mañas, T. Parella, J. Benet-Buchholz, *J. Org. Chem.*, **2005**, *70*, 2033; b) S. Brun, L. Garcia, I. González, A. Torrent, A. Dachs, A. Pla-Quintana, T. Parella, A. Roglans, *Chem. Commun.*, **2008**, 4339; c) I. González, A. Pla-Quintana, A. Roglans. *Synlett*, **2009**, 2844; d) L. Garcia, A. Pla-Quintana, A. Roglans, T. Parella. *Eur. J. Org. Chem.*, **2010**, 3407; e) S. Brun, M. Parera, A. Pla-Quintana, A. Roglans, T. Leon, T. Achard, J. Solà, X. Verdaguer, A. Riera, *Tetrahedron*, **2010**, *66*, 9032; f) A. Dachs, A. Pla-Quintana, T. Parella, M. Solà, A. Roglans. *Chem. Eur. J.*, **2011**, *17*, 14493; g) S. Brun, A. Torrent, A. Pla-Quintana, A. Roglans, X. Fontrodona, J. Benet-Buchholz, T. Parella, *Organometallics*, **2012**, *31*, 318; h) T. León, M. Parera, A. Roglans, A. Riera, X. Verdaguer. *Angew. Chem. Int. Ed.*, **2012**, *51*, 6851; i) E. Haraburda, A. Lledó, A. Roglans, A. Pla-Quintana, *Org. Lett.* **2015**, *17*, 2882.

[9] For selected references, see: a) S. –I, Ikeda; Watanabe, H.; Sato, Y. *J. Org. Chem.* **1998**, *63*, 7026; b) Itooka, R. Y. Iguchi, N. Miyaura, *J. Org. Chem.* **2003**, *68*, 6000; c) K. Tanaka, K. Ajiki, *Org. Lett.* **2005**, *7*, 1537. (d) M. G. Musolino, G. Apa, A. Donato, R. Pietropaolo, *Catal. Today* **2005**, *100*, 467. (e) G. Lalic; E. Corey, J. *Tetrahedron Lett.* **2008**, *49*, 4894.

[10] For selected references of DFT studies catalysed by Rh, see: a) L. Orian, J. N. P. van Stralen, F. M. Bickelhaupt, *Organometallics* **2007**, *26*, 3816–3830; b) A. Dachs, A. Torrent, A. Roglans, T. Parella, S. Osuna, M. Solà, *Chem. Eur. J.* **2009**, *15*, 5289; c) A. Dachs, S. Osuna, A. Roglans, M. Solà, *Organometallics* **2010**, *29*, 562; d) A. Dachs, A. Roglans, M. Solà, *Organometallics* **2011**, *30*, 3151; e) A. Dachs, A. Pla-Quintana, T. Parella, M. Solà, A. Roglans, *Chem. Eur. J.* **2011**, *17*, 14493; f) L. Orian, M. Swart, F. M. Bickelhaupt, *ChemPhysChem* **2014**, *15*, 219.; g) Ò. Torres, A. Roglans, A. Pla-Quintana, J. M. Luis, M. Solà, *J. Organomet. Chem.* **2014**, *768*, 15.

[11] N. E. Schore, *Chem. Rev.* **1988**, *88*, 1081–1119.

[12] T. A. Albright, J. K. Burdett and M.-H. Whangbo, *Orbital Interaction in Chemistry*, John Wiley & Sons, New York, 1985.

[13] a) S. Kozuch, S. Shaik, *J. Am. Chem. Soc.* **2006**, *128*, 3855-3365; b) S. Kozuch, S. Shaik, *J. Phys. Chem. A.* **2008**, *112*, 6032-6041; c) S. Kozuch, S. Shaik, *Acc. Chem. Res.* **2011**, *44*, 101-110.

[14] For selected references on detection and isolation of intermediates, see: a) H. Nishiyama, E. Niwa, T. Inoue, Y. Ishima, K. Aoki, *Organometallics* **2002**, *21*, 2572; b) A. Dachs, A. Torrent, A. Pla-Quintana, A. Roglans, A. Jutand, *Organometallics* **2009**, *28*, 6036; c) B. Dutta, B. F. E. Curchod, P. Campomanes, E. Solari, R. Scopelliti, U.Rothlisberger, K. Severin, *Chem. Eur. J.* **2010**, *16*, 8400; d) M. Parera, A. Dachs, M. Solà, A. Pla-Quintana, A. Roglans, *Chem. Eur. J.* **2012**, *18*, 13097; e) G. Bottari, L. L. Santos, C. M. Posadas, J. Campos, K. Mereiter, M. Paneque, *Chem. Eur. J.* **2016**, *22*, 13715.

[15] Since no species could be detected upon injection of $[RhCl(CO)_2]_2$ into the mass spectrometer, different additives were tested. Addition of a methanolic solution of LiCl proved to be highly efficient for the detection of chloride adducts in the negative ion mode.

[16] a) Z-X. Yu, P.A. Wender, K.N. Houk, *J. Am. Chem. Soc.* **2004**, *126*, 9154-9155; b) P. Liu, P.H-H. Cheong, Z-X. Yu, P.A. Wender, K.N. Houk, *Angew. Chem. Int. Ed.* **2008**, *47*, 3939-3941; c) Z.-X. Yu, P.H.-Y. Cheong, P. Liu, C.Y. Legauld, P.A. Wender, K.N. Houk, *J. Am. Chem. Soc.* **2008**, *130*, 2378-2379; d) P. Liu, L.E. Sirois, P.H.-Y. Cheong, Z.-X. Yu, I.V. Hartung, H. Rieck, P.A. Wender, K.N. Houk, *J. Am. Chem. Soc.* **2010**, *132*, 10127-10135; e) X. Xu, P. Liu, A. Lesser, L.E. Sirois, P.A. Wender, K.N. Houk, *J. Am. Chem. Soc.* **2012**, *134*, 11012-11025; f) X. Hong, M.C. Stevens, P. Liu, P.A. Wender, K.N. Houk, *J. Am. Chem. Soc.* **2014**, *136*, 17273-17283; g) T.J.L. Mustar, P.A. Wender, P.H.-Y. Cheong, *ACS Catal.* **2015**, *5*, 1758-1763.

[17] a) A. W. Ehlers, S. Dapprich, S. F. Vyboischchikov, G. Frenking, *Organometallics* **1996**, *15*, 105-117; b) A. Kovacs, G. Frenking, *Organometallics* **2001**, *20*, 2510-2524.

[18] a) A. D. Becke, *J. Chem. Phys.* **1993**, *98*, 5648-5652; b) C. Lee, W. Yna,g R. G. Parr, *Phys. Rev. B* **1988**, *37*, 785-789; c) P. J. Stephens, F. J. Devlin, C. F. Chabalowski, M. J. Frisch, *J. Phys. Chem.* **1994**, *98*, 11623-11627.

[19] a) T. H. Dunning, Jr., *J. Chem. Phys.* **1989**, *90*, 1007-1023; b) D. E. Woon, T. H. Dunning, Jr., *J. Chem. Phys.* **1993**, *98*, 1358-1371.

[20] K. A. Peterson, D. Figgen, M. Dolg, H. Stoll, *J. Chem. Phys.* **2007**, *126*, 124101.

[21] S. Grimme, J. Antony, S. Ehrlich and H. Krieg, *J. Chem. Phys.* **2010**, *132*, 154104.

[22] P. Atkins, J. De Paula in *Physical Chemistry*, Oxford University Press, Oxfor **2006**.

[23] C. Gonzalez, H. B. Schlegel, *J. Chem. Phys.* **1989**, *90*, 2154-2161.

[24] M. J. Frisch, G. W. Trucks, H. B. Schlegel, G. E. Scuseria, M. A. Robb, J. R Cheeseman, G. Scalmani, V. Barone, B. Mennucci, G. A. Petersson, H Nakatsuji, M. Caricato, X. Li, H. P. Hratchian, A. F. Izmaylov, J. Bloino, G Zheng, J. L. Sonnenberg, M. Hada, M. Ehara, K. Toyota, R. Fukuda, J Hasegawa, M. Ishida, T. Nakajima, Y. Honda, O. Kitao, H. Nakai, T. Vreven, J A. Montgomery Jr., J. E. Peralta, F. Ogliaro, M. Bearpark, J. J. Heyd, E Brothers, K. N. Kudin, V. N. Staroverov, R. Kobayashi, J. Normand, K Raghavachari, A. Rendell, J. C. Burant, S. S. Iyengar, J. Tomasi, M. Cossi, N Rega, J. M. Millam, M.Klene, J. E. Knox, J. B. Cross, V. Bakken, C. Adamo, J Jaramillo, R. Gomperts, R. E. Stratmann, O. Yazyev, A. J. Austin, R. Cammi, C Pomelli, J. W. Ochterski, R. L. Martin, K. Morokuma, V. G. Zakrzewski, G. A Voth, P. Salvador, J. J. Dannenberg, S. Dapprich, A. D. Daniels, Ö. Farkas, J. B Foresman, J. V. Ortiz, J. Cioslowski, D. J. Fox, Gaussian 09, revision E.0 Gaussian, Inc., Pittsburg, PA, **2009**.

[25] a) L. Orian, L. P. Wolters and F. M. Bickelhaupt, *Chem. Eur. J.* **2013**, *1* 13337; b) C.-H. Guo, H.-S. Wu, M. Hapke and H. Jiao, *J. Organomet. Chem* **2013**, *748*, 29.

Received: ((will be filled in by the editorial staff
Revised: ((will be filled in by the editorial staff
Published online: ((will be filled in by the editorial staff

10.1002/chem.201703194

Entry for the Table of Contents

Cycloaddition

Daniel Cassú, Teodor Parella, Miquel Solà, Anna Pla-Quintana* and Anna Roglans**.... Page – Page

Rhodium-catalysed [2+2+2] cycloaddition reactions of linear allene-ene-ynes to afford fused tricyclic scaffolds. Insights into the mechanism

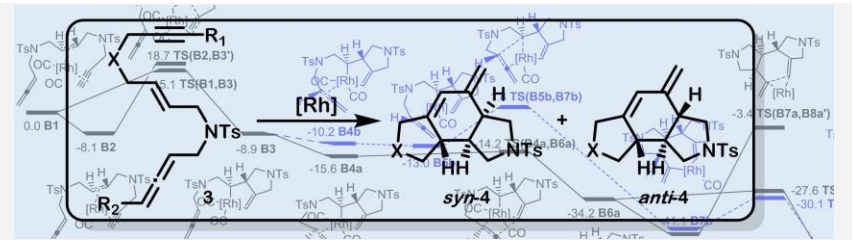

Fused tricyclic scaffolds: The three carbon based-unsaturations (allene-alkyne-allene) have been jointly involved in a [2+2+2] cycloaddition reaction under rhodium catalysis. The ligands on the catalyst affect the diastereoselectivity of the process. DFT calculations rationalizes these selectivity issues and the order in which the different insaturations take part in the catalytic cycle.